Influence of a centered dielectric tube on inductively coupled plasma source: Chamber structures and plasma characteristics*

Zhen-Hua Bi(毕振华)[1], Yi Hong(洪义)[1], Guang-Jiu Lei(雷光玖)[2], Shuai Wang(王帅)[3], You-Nian Wang(王友年)[4], and Dong-Ping Liu(刘东平)[1,†]

[1] *Liaoning Key Laboratory of Optoelectronic Films & Materials, School of Physics and Materials Engineering, Dalian Nationalities University, Dalian* 116600, *China*

[2] *Southwestern Institute of Physics, Chengdu* 610041, *China*

[3] *Physics Department, School of Science, Northeastern University, Shenyang* 110819, *China*

[4] *School of Physics and Optoelectronic Technology, Dalian University of Technology, Dalian* 116024, *China*

(Received 30 November 2016; revised manuscript received 13 March 2017; published online 6 June 2017)

A high-density RF ion source is an essential part of a neutral beam injector. In this study, the authors attempt to retrofit an original regular RF ion source reactor by inserting a thin dielectric tube through the symmetric axis of the discharge chamber. With the aid of this inner tube, the reactor is capable of generating a radial magnetic field instead of the original transverse magnetic field, which solves the $E \times B$ drift problem in the current RF ion source structure. To study the disturbance of the dielectric tube, a fluid model is introduced to study the plasma parameters with or without the internal dielectric tube, based on the inductively coupled plasma (ICP) reactor. The simulation results show that while introducing the internal dielectric tube into the ICP reactor, both the plasma density and plasma potential have minor influence during the discharge process, and there is good uniformity at the extraction region. The influence of the control parameters reveals that the plasma densities at the extraction region decrease first and subsequently slow down while enhancing the diffusion region.

Keywords: neutral beam ion source, inductively coupled plasma (ICP), fluid model

PACS: 52.65.–y, 52.50.Dg **DOI:** 10.1088/1674-1056/26/7/075203

1. Introduction

Neutral beam injection (NBI) is one of the most essential ways of heating fusion plasmas in TOKAMAK and has been developed rapidly in recent years.[1–3] In 2007, ITER selected a radio-frequency (RF)-driven ion source instead of the original filament source.[4] The heating system requires a reliable negative ion source providing high current density (> 200 A·m^{-2}) with high uniformity and at low pressure < 0.3 Pa.[5] It hence needs a high-density, large-area plasma source with good uniformity. At present, the negative RF ion source is a solenoidal coiled inductively coupled plasma (ICP) reactor developed at IPP (Max Planck Institut für Plasmaphysik), Garching.[6,7] Compared with the former filamented arc sources, the greatest advantage of the present source is that it can endure longer operating times owing to the absence of filaments, and this has attracted increasing attention for basic physics investigation and device optimization.[8–13]

However, some research groups indicate that there exists a major problem based on the current structure: while adding an external (horizontal) magnetic filter perpendicular to the cylindrical axis, the axial electric field and the horizontal magnetic field will lead to an $E \times B$ drift of the electrons,[8,9] leading to a 'Hall effect', whereby the potential is no longer axially symmetric. The potential at one side of the chamber (towards the $E \times B$ direction) is larger than at the opposite side. Then, the radial potential drop will accordingly cause a secondary drift to extract the electrons from the confined magnetic field. As a result, this will cause radial nonuniformity of the plasma density and also strongly affect the production of H negative ions by the extracted electron flux. Detailed descriptions of the simulation and experimental work can be found in Refs. [8]–[12].

Since the main cause of this problem is the Hall effect induced by the horizontal magnetic field, we consider changing the static magnetic field configuration to avoid this Hall effect. Therefore, based on the original ICP source structure, we insert a thin tube into the chamber along the axial direction. The magnet could be placed inside the dielectric tube to generate a radial magnetic field. Thus, the $E \times B$ drift becomes a closed drift without hitting the wall. This may be one possible solution for RF source reactor optimization. For a planar coil ICP, this reactor geometry was first developed by Ventzek *et al.* as a step window to investigate the distributions of the plasma parameters.[13] For a solenoidal coil ICP, Monreal *et al.* designed a cylindrically symmetric ICP reactor with inner antenna coils to demonstrate the control of electron temperature and electron energy distribution (EED) in low-pressure ICP.[14] Song *et al.* employed a hybrid model to compare with

*Project supported by the National Natural Science Foundation of China (Grant Nos. 11305028, 11305032, and 11320101005).

†Corresponding author. E-mail: dongping.liu@dlnu.edu.cn

© 2017 Chinese Physical Society and IOP Publishing Ltd

the above experimental measurement results to investigate the static magnetic effects on the EEDs.[15] All of the above results indicate that the shape of an ICP chamber structure will not cause a disturbance of the plasma discharge. However, it still requires a comparison, particularly under extremely high power and for a specific structure.

Except for its use as an ion source, the solenoidal coil ICP source is also widely applied in many other low-pressure plasma discharge environments, such as semiconductor fabrication facilities. A thorough investigation is necessary to understand both the properties of the plasma parameters and also the influence of the controlled parameters on the discharge status, which will provide valuable guidance for the design of the source reactor. In order to test the feasibility of the new structure, a fluid simulation is introduced based on this geometry to investigate the plasma density, potential, and electron temperature distributions, as well as the influence of the applied power and reactor geometry. A simulation based on the original regular chamber geometry under the same discharge status is also conducted for comparison. It needs to be mentioned that this paper will mainly focus on the effect of geometry on the inductive heating mechanics. The effect of the static magnetic field is not taken into consideration in the current study.

2. Chamber design

The schematic of the RF source geometry is shown in Fig. 1. Figure 1(a) shows a regular solenoidal coil ICP configuration. Figure 1(b) shows our newly retrofitted structure, in which a hollow thin tube is inserted into the RF source along the axial direction. In this way, the static magnets can be placed in the inner tube to generate a radial magnetic field. We divide each of them into two parts: the upper half is the discharge region and the lower half is the diffusion region.

The simulation area is shown on the right-hand side of Fig. 1. The chamber reactor is set to 420 mm in height with a radius of 120 mm. The coils are located in the upper part of the chamber. Thus, the entire chamber can be divided into two parts: the discharge region (upper half) and the diffusion region (lower half). In order to limit the disturbance to the plasma discharge, we set the radius of the inner tube as 20 mm. The distance from the reactor bottom to the inner tube bottom is 60 mm. We take helium as the carrier gas and fix the gas pressure at 10 mTorr. The coil is connected to a 2 MHz RF source with available input power from 1 to 100 kW.

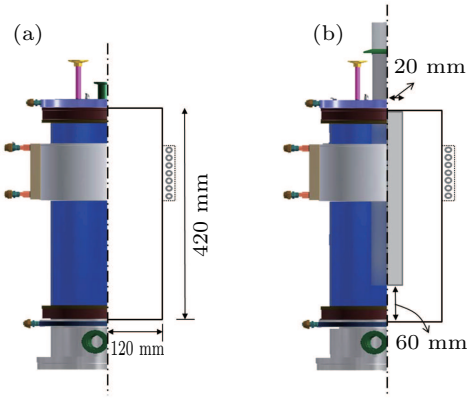


Fig. 1. (color online) Schematic view of the reactor geometry: (a) regular solenoidal coil ion source reactor and (b) new retrofitted source reactor.

3. Numerical model

A fluid model is employed to simulate the discharge status in both the regular geometry and new geometry. The fluid method is widely used for the simulation of low-temperature plasma sources.[13,15–21] Model descriptions and numerical methods can be found in our earlier work.[16] The code we employed in this paper is a part of the MAPS (Multi-physics Analysis for Plasma Simulation) solver. MAPS is a comprehensive solver developed by Wang's group.[22] It consists of CCP and ICP solvers. One can select a fluid model or particle-in-cell (PIC) model for simulating the CCP discharge. For ICP discharge, only the fluid model is available, temporarily. A number of experimental verifications have been conducted and the simulation results show good agreement with the corresponding experimental results, for both CCP and ICP discharges.[23,24] This solver could effectively deal with various reactive gases, such as H_2, He, N_2, O_2, Ar, CF_4, and SiH_4, among others, as well as gas mixtures. In this study, we selected some of the main reactions of He plasma discharge, including ionization, excitation, de-excitation, multistep ionization, and three-body interactions, among others. The reactions and rate coefficients are listed in Table 1.

Table 1. Rate coefficients for He plasma in $cm^{-3}\cdot s^{-1}$ ($cm^{-6}\cdot s^{-1}$ for three-body collisional reaction); ε_j is the threshold energy, T_e is the electron temperature in eV, and T_n is the background gas temperature in eV.

No.	Reaction	ε_j	Rate coefficient	Reference
1	$e + He \rightarrow e + He$		cross-section[a]	[17], [18]
2	$e + He \rightarrow e + He^*$	19.8	cross-section[a]	[17], [18]
3	$e + He^* \rightarrow e + He$	–19.8	cross-section[a]	[17], [18]
4	$e + He \rightarrow 2e + He^+$	24.6	cross-section[a]	[17], [18]
5	$e + He^* \rightarrow 2e + He^+$	4.8	cross-section[a]	[17], [18]
6	$2e + He^+ \rightarrow e + He^*$		$6.0\times10^{-20}\,(T_e/T_n)^{-4.4}$	[18]
7	$e + He^+ + He \rightarrow He + He^*$		$1.0\times10^{-26}\,(T_e/T_n)^{-2}$	[18]
8	$He^* + He^* \rightarrow e + He + He^+$		$8.7\times10^{-10}\,(T_n/0.0025)^{0.5}$	[18]

[a]Calculated by Boltzmann equation.

The set of fluid equations includes the continuity equation for ion/electron density

$$\frac{\partial n_{\mathrm{i,e}}}{\partial t} + \nabla \cdot \boldsymbol{\Gamma}_{\mathrm{i,e}} = S_{\mathrm{i,e}}, \tag{1}$$

the momentum balance and drift–diffusion equations for ion/electron flux

$$\frac{\partial \boldsymbol{u}_{\mathrm{i}}}{\partial t} + \boldsymbol{u}_{\mathrm{i}} \boldsymbol{\nabla} \cdot \boldsymbol{u}_{\mathrm{i}} = -\boldsymbol{\nabla} P_{\mathrm{i}} + \frac{e\boldsymbol{E}}{m_{\mathrm{i}}} - \nu_{\mathrm{i}} \boldsymbol{u}_{\mathrm{i}}. \tag{2}$$

$$\boldsymbol{\Gamma}_{\mathrm{e}} = -\frac{1}{m_{\mathrm{e}} \nu_{\mathrm{e}}} \boldsymbol{\nabla} (n_{\mathrm{e}} T_{\mathrm{e}}) - \frac{e n_{\mathrm{e}}}{m_{\mathrm{e}} \nu_{\mathrm{e}}} \boldsymbol{E}, \tag{3}$$

and energy balance equation for electron energy (temperature)

$$\frac{\partial \left(\frac{3}{2} n_{\mathrm{e}} k_{\mathrm{B}} T_{\mathrm{e}}\right)}{\partial t} = -\boldsymbol{\nabla} \cdot \boldsymbol{q}_{\mathrm{e}} - e\boldsymbol{E} \cdot \boldsymbol{\Gamma}_{\mathrm{e}} - \sum \varepsilon_j k_j N n_{\mathrm{e}} + P_{\mathrm{abs}}. \tag{4}$$

For the neutral particles, we consider only the diffusion function (Fick's law)

$$\frac{\partial n_{\mathrm{n}}}{\partial t} - D_{\mathrm{n}} \boldsymbol{\nabla}^2 n_{\mathrm{n}} = S_{\mathrm{n}}. \tag{5}$$

Here, $n_{\mathrm{i,e}}$ and n_{n} represent the density of ions, electrons, and excited He atoms. $\boldsymbol{\Gamma}_{\mathrm{i,e}}$ represents the ion and electron fluxes. $P_{\mathrm{i}} = n_{\mathrm{i}} k_{\mathrm{B}} T_{\mathrm{i}}$ is the ion pressure and T_{i} is the ion temperature. Here, we set the ion temperature equal to the background gas temperature T as a constant value of 300 K. For the electron energy balance equation, P_{abs} is the absorption power and the energy flux $\boldsymbol{q}_{\mathrm{e}}$ is expressed as

$$\boldsymbol{q}_{\mathrm{e}} = \frac{5}{2} k_{\mathrm{B}} T_{\mathrm{e}} \boldsymbol{\Gamma}_{\mathrm{e}} - \frac{5}{2} \frac{n_{\mathrm{e}} k_{\mathrm{B}} T_{\mathrm{e}}}{m_{\mathrm{e}} \nu_{\mathrm{e}}} \boldsymbol{\nabla} (k_{\mathrm{B}} T_{\mathrm{e}}).$$

$S_{\mathrm{i,e}}$ and S_{n} represent the source item in the form of $S_{\mathrm{i,e}} = \sum k_{\mathrm{pro}} n_1 n_2 - \sum k_{\mathrm{rea}} n_1 n_2$. k_{pro} and k_{rea} are the rate coefficients of the reactions for the product or reactant and $n_{1,2}$ are the reactants for each reaction. The energy losses of ionization and excitation ε_{j} are also listed in Table 1. In order to satisfy the Courant condition, the maximum grid size is 300 × 420 and the time step is set to approximately 2000 steps per RF period.

In this model, we approximate the temperature of the background gas as the room temperature. In fact, the background gas temperature could be heated up to more than 1000 K owing to low-pressure and high-power discharge.[25] According to the ideal gas equation $P = N k_{\mathrm{B}} T$, it can be deduced that if the simulated gas temperature is lower than the real temperature, the computed neutral particle number density will be larger than the actual value. Therefore, strictly speaking, the simulated results for the plasma density are higher owing to this approximation. However, the advantage of the existing model is its computing speed: it will cost only a few hours without the neutral gas thermo-fluid module.

4. Results and discussion

4.1. Comparisons to the original reactor

Figures 2(a) and 2(b) show the electron density distributions in the regular and new chamber geometries, respectively. Regarding the new configuration, the main problem may be the magnitude of the plasma density. To achieve a high-power ion flux, we need to generate high-density plasmas in the reactor. As shown in the figure, the peak value of the He plasma density can reach 10^{18} m^{-3} at an input power of 50 kW and pressure of 10 mTorr. Comparing the two situations above, in the discharge region, the peak density shows only a slight decrease in this new reactor. The ionization rates (which are not shown in the figure) in the density peak region are nearly identical. It can be deduced that the axial inner tube does not significantly affect the electron heating. The heating mechanism is mostly due to the angular electric field, with little impact on the radial direction. Furthermore, in the diffusion region, the electron heating effect became more obvious in the original structure. This is because in the new structure, the electrons are more likely to lose by hitting the wall of inner tube.

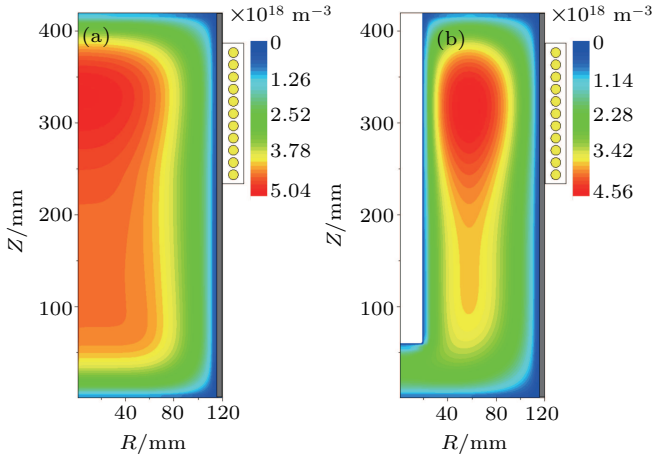


Fig. 2. (color online) Comparison of the time-averaged electron density distribution between (a) regular discharge chamber and (b) new retrofitted discharge chamber with an inner tube (blank area on the left side).

The radial distribution of the plasma density at the bottom is presented in Fig. 3. In both cases, the plasma density shows good radial uniformity. The requirement of ITER for the radial uniformity is approximately 90%. In both structures, this requirement could cover the individual radial ranges of 76 mm and 71 mm. This is sufficient for the subsequent work on ion extraction.[26] In the expansion region, the density distribution is mainly caused by the diffusion progress. ICP discharge possesses a rather thin plasma sheath, so that the distance between the bottom of the tube and the reactor is much larger than the plasma sheath. To conclude, the inner tube has minor influence on the plasma density in the extraction region.

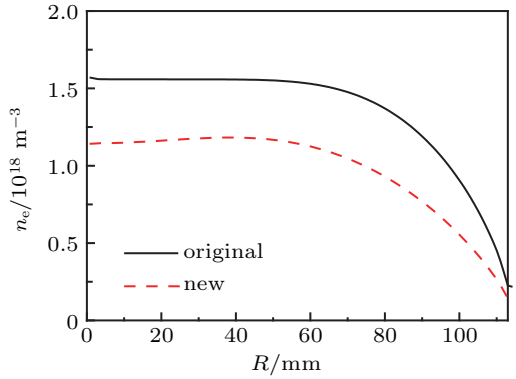


Fig. 3. (color online) Radial distributions of the electron densities at the bottom part of the source reactor. The black line shows the electron density in original regular chamber (Fig. 1(a)) and the red dashed line shows the case in the new retrofitted chamber (Fig. 1(b)).

Figure 4 shows the comparison of the plasma potential distribution. In both configurations, the plasma potential is maintained in the range of approximately 20 V. There exists a potential gradient along the vertical direction, which contributes the $E \times B$ drift as the source of the electric field. Similar to the electron density distribution, in the new geometry, the inserted inner tube also has minor influence on the potential in the plasma region, and a thin sheath is formed around the outer tube.

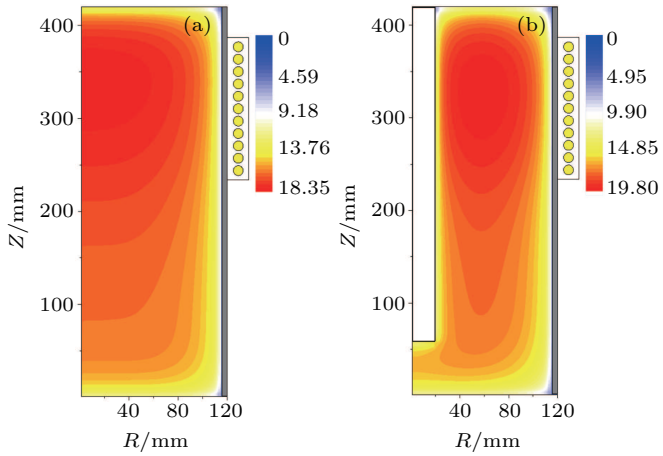


Fig. 4. (color online) Comparison of the time-averaged plasma potential distribution (in units of V) between (a) regular discharge chamber and (b) new retrofitted discharge chamber with an inner tube (the blank area in left side).

4.2. Influence of the control parameters

As we know, the discharge status is directly affected by the applied power. Considering the high-power condition, the absorption power is increased from 1 kW to 100 kW. We selected the conditions of 5 kW and 50 kW in Fig. 5. It can be seen from the figure that the areas of the high-density peaks are essentially the same. In the case of extremely high supplied power (Fig. 5(b)), electrons in the diffusion region are more likely to be affected by the source heating. This effect leads to a higher plasma density in the bottom half of the chamber.

The averaged ion flux density at the bottom and the plasma peak density versus the applied power are shown in Fig. 6. We see that the ion flux and plasma peak density exhibit linear behavior with respect to the applied power from 1 kW to 100 kW. From the energy balance equation (Eq. (4)), we see that when the value of the absorption power is large enough, it will play a major role on the right side of the equation. Thus, the electron energy $n_e T_e$ becomes linear with respect to the absorption power. The variation of the electron temperature does not change significantly, leading to a linear relationship between the electron density and the applied power. In the lower applied power regime, this relationship will be made more nonlinear by the contributions of heat conduction and convection. In addition, the ICP source could also be used to investigate high-energy ion irradiation. Analyzing the relationship between the input power and ion flux will be helpful to study the irradiation damage in different power supplies.

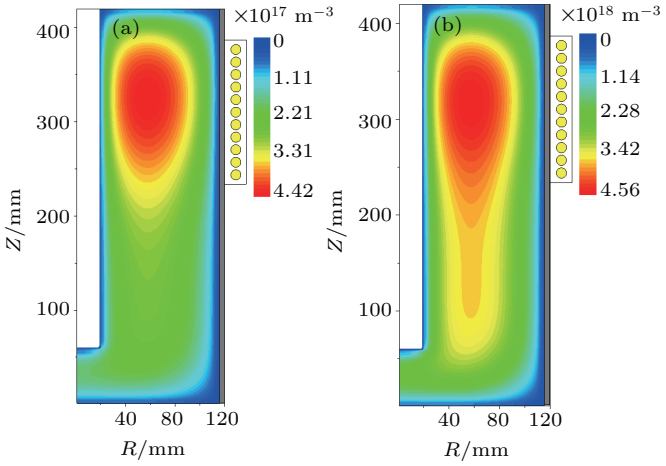


Fig. 5. (color online) Time-averaged distributions of the electron density in different applied power: (a) 5 kW and (b) 50 kW.

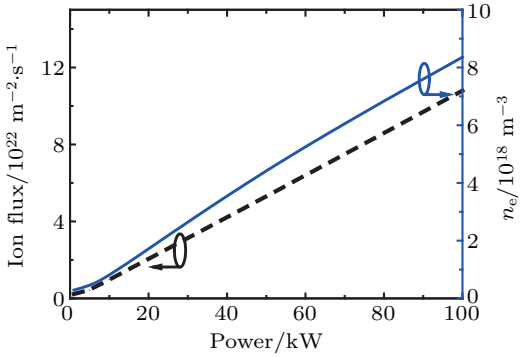


Fig. 6. (color online) Attracted ion flux (black dashed line) and plasma peak density (blue line) under different applied power.

Seeing that the plasma density in the expansion region is approximately half of the peak density value, we try to test the effect of diffusion length on plasma density. In this simulation, the discharge region and the bottom outflow part are fixed, and we gradually decrease the diffusion length. It seems that decreasing the diffusion length could considerably enhance the plasma density in the bottom region. In fact, however, as

shown in Fig. 7, the value of the bottom plasma density looks almost the same, though the diffusion length has already reduced to near zero (Fig. 7(c)). When we shorten the diffusion length, the overall plasma density shows a slight increase because of the compression of the whole chamber area. To get a clearer view, figure 8 shows the bottom electron density for different diffusion lengths with the powers of 5 kW and 50 kW. Both cases show that when we shorten the diffusion length, the plasma density does not change significantly at first and then increases when the diffusion region is small enough. This may show us that in most cases, there is no need to diminish the diffusion region to seek a higher extraction of the plasma density.

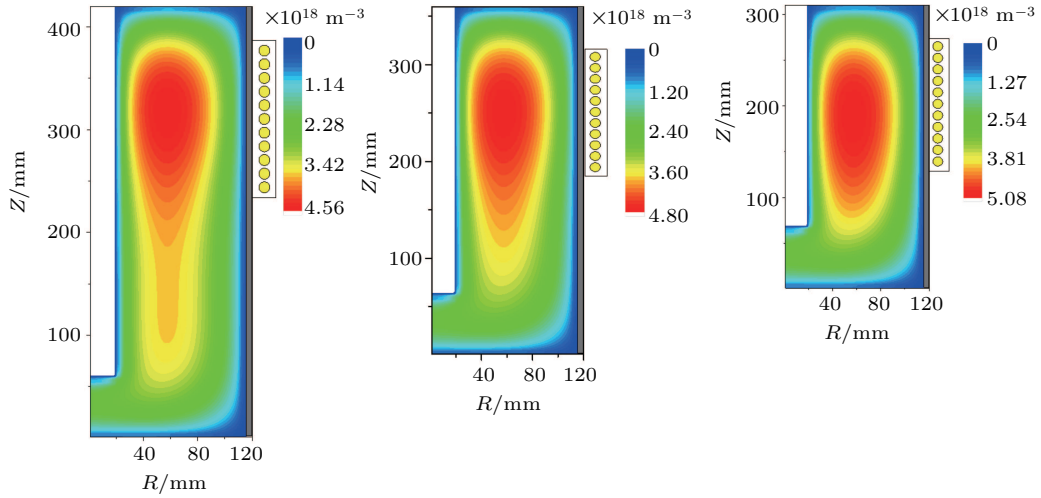


Fig. 7. (color online) (a)–(c) Time-averaged distributions of the electron density in different geometry configurations.

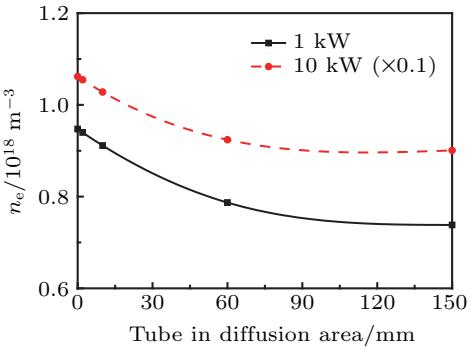


Fig. 8. (color online) Bottom electron density varies with the length of the diffusion area under the power of 5 kW (black line) and 50 kW (red dashed line).

5. Conclusion

A new reactor geometry is proposed for the optimization of an RF ion source. The purpose of this design is to change the original transverse magnetic field to a radial magnetic field by introducing a centered dielectric tube into the RF ICP chamber. For the first step, we simulate the physical influence of the dielectric tubes without introducing the static magnetic field and negative ions. A fluid model is introduced to simulate the discharge status under this new reactor geometry. The results reveal that the inner tube causes only a minor decrease in the plasma density. The radial distribution of the plasma density in the extraction region maintains good uniformity, both with and without the inner tube. The influence of the control parameters shows that both the ion flux and the plasma density show linear behavior with respect to the applied power under high-input-power conditions (1–100 kW). In the extraction region, longer diffusion length causes less influence on the plasma density. In summary, the disturbance by the inserted dielectric tube of the plasma density and radial uniformity can be ignored. Owing to its advantage of generating the radial magnetic field, this new chamber geometry could be a practical way to optimize the current RF negative ion source structure.

Acknowledgements

The authors would like to thank Prof. Jean-Pierre Boeuf for the ideas and discussions regarding this work.

References

[1] Hemsworth R, Decamps H, Graceffa J, Schunke B, Tanaka M, Dremel M, Tanga A, DeEsch H P L, Geli F, Milnes J, Inoue T, Marcuzzi D, Sonato P and Zaccaria P 2009 *Nucl. Fusion* **49** 045006

[2] Hu C D, Xu Y J, Xie Y L, Liu S, Liu Z M, Sheng P, Xie Y H and Liang L Z 2015 *Chin. Phys. Lett.* **32** 052901

[3] Cao J Y, Wei H L, Zou G Q, Liu H, Lei G J, Zhang X M, Yang X F, Yu L M, Jiang T, Jiang S F and Rao J 2013 *Fusion Eng. Des.* **88** 872

[4] Hemsworth R S, Tanga A and Antoni V 2008 *Rev. Sci. Instrum.* **79** 02C109

[5] Hemsworth R S and Inoue T 2005 *IEEE Trans. Plasma Sci.* **33** 1799

[6] Fantz U, Franzen P, Kraus W, Berger M, Christ-Koch S, Fröschle M, Gutser R, Heinemann B, Martens C, McNeely P, Riedl R, Speth E and Wünderlich D 2007 *Plasma Phys. Control. Fusion* **49** B563

[7] Speth E, Falter H D, Franzen P, Fantz U, Bandyopadhyay M, Christ S, Encheva A, Fröschle M, Holtum D, Heinemann B, Kraus W, Lorenz A, Martens Ch, McNeely P, Obermayer S, Riedl R, Süss R, Tanga A, Wilhelm R and Wünderlich D 2006 *Nucl. Fusion* **46** S220

[8] Hagelaar G J M and Oudini N 2011 *Plasma Phys. Control. Fusion* **53** 124032

[9] Boeuf J P, Hagelaar G J M, Sarrailh P, Fubiani G and Kohen N 2011 *Plasma Sources Sci. Technol.* **20** 015002
[10] Fubiani G and Boeuf J P 2014 *Phys. Plasmas* **21** 073512
[11] Gaboriau F, Baude R and Hagelaar G J M 2014 *Appl. Phys. Lett.* **104** 214107
[12] Schiesko L, Franzen P and Fantz U 2012 *Plasma Sources Sci. Technol.* **21** 065007
[13] Ventzek P L G, Grapperhaus M and Kushner M J 1994 *J. Vac. Sci. Technol. B* **12** 3118
[14] Arancibia Monreal J, Chabert P and Godyak V 2013 *Phys. Plasmas* **20** 103504
[15] Song S H, Yang Y, Chabert P and Kushner M J 2014 *Phys. Plasmas* **21** 093512
[16] Bi Z H, Dai Z L, Zhang Y R, Liu D P and Wang Y N 2013 *Plasma Sources Sci. Technol.* **22** 055007
[17] Morgan W L *Kinema Research and Software*, *LXcat database*
[18] Van Laer K and Bogaerts A 2016 *Plasma Sources Sci. Technol.* **25** 015002
[19] Hagelaar G J M, Fubiani G and Boeuf J P 2011 *Plasma Sources Sci. Technol.* **20** 015001
[20] Ventzek P L G, Hoekstra R J and Kushner M J 1994 *J. Vac. Sci. Technol. B* **12** 461
[21] Stewart R A, Vitello P and Graves D B 1994 *J. Vac. Sci. Technol. B* **12** 478
[22] Zhang Y R, Gao F, Li X C, Bogaerts A and Wang Y N 2015 *J. Vac. Sci. Technol. A* **33** 061303
[23] Bi Z H, Dai Z L, Xu X, Li Z C and Wang Y N 2009 *Phys. Plasmas* **16** 043510
[24] Xu H J, Zhao S X, Gao F, Zhang Y R, Li X C and Wang Y N 2015 *Chin. Phys. B* **24** 115201
[25] Hebner G A 1996 *J. Appl. Phys.* **80** 2624
[26] Franzen P, Falter H, Heinemann B, Martens Ch, Fantz U, Berger M, Christ-Koch S, Fröschle M, Holtum D, Kraus W, Leyer S, McNeely P, Riedl R, Süss R, Obermayer S, Speth E and Wünderlich D 2007 *Fusion Eng. Des.* **82** 407